Astronomy & Astrophysics manuscript no. GRB111117A
Wednesday 24th May, 2017

The host galaxy of the short GRB 111117A at z = 2.211. ⋆

J. Selsing[1], T. Krühler[2], D. Malesani[1,3], P. D'Avanzo[4], J. Palmerio[5], S. D. Vergani[6], J. Japelj[6], B. Milvang-Jensen[1], D. Watson[1], P. Jakobsson[7], Z. Cano[8], J. P. U. Fynbo[1], A. Gomboc[9], K. E. Heintz[7,1], M. Sparre[1,10], and XSGRB collaboration

[1] Dark Cosmology Centre, Niels Bohr Institute, University of Copenhagen, Juliane Maries Vej 30, 2100 København Ø, Denmark
[2] Max-Planck-Institut für extraterrestrische Physik, Giessenbachstraße, 85748 Garching, Germany
[3] DTU Space, National Space Institute, Technical University of Denmark, Elektrovej 327, DK-2800 Lyngby, Denmark
[4] INAF - Osservatorio Astronomico di Brera, via E. Bianchi 46, I-23807, Merate (LC), Italy
[5] Sorbonne Universités, UPMC Univ. Paris 6 et CNRS, UMR 7095, Institut d'Astrophysique de Paris, 98 bis bd Arago, 75014 Paris, France
[6] GEPI, Observatoire de Paris, PSL Research University, CNRS, Univ. Paris Diderot, Sorbonne Paris Cité, 5 Place Jules Janssen, 92195 Meudon, France
[7] Centre for Astrophysics and Cosmology, Science Institute, University of Iceland, Dunhagi 5, 107 Reykjavík, Iceland
[8] Instituto de Astrofísica de Andalucía (IAA-CSIC), Glorieta de la Astronomía s/n, E-18008, Granada, Spain.
[9] University of Nova Gorica, Vipavska 13, 5000 Nova Gorica, Slovenia.
[10] Heidelberger Institut für Theoretische Studien, Schloss-Wolfsbrunnenweg 35, 69118 Heidelberg, Germany

Received/ accepted

ABSTRACT

Short γ-ray bursts (sGRBs) and their hosts are notoriously difficult to localize. We here present evidence of the, to date, highest redshift high-confidence short GRB, located at $z = 2.211$. This value supersedes a previously estimated, lower redshift value. Spectroscopic observations along with a wealth of imaging data allow us to place tight constraints on the nature of the host galaxy at an unprecedented distance. The rest frame X-ray derived hydrogen column density is high compared to a complete sample of sGRBs and seems to follow the evolution with redshift as traced by the hosts of long GRBs (lGRBs). This could indicate that the part of the sGRB population hosted in late-type galaxies, live in similar environments to that of lGRB hosts. The host is in the brighter end of the expected host brightness distribution at $z = 2.211$, but only 30 per cent of the distribution should be missed due to host faintness at this redshift. This indicates that we are not missing redshifts for a dominant fraction of the sGRB hosts at this redshift. The redshift of GRB111117A is evidence against a lognormal delay-time model for sGRBs through the predicted redshift distribution of sGRBs, which is very sensitive to high-z sGRBs. From the age of the universe at explosion time, an initial progenitor separation of $a_0 < 3.2 R_\odot$ is required for the case of a binary neutron star (NS) system. It puts constraints on the progenitor system evolution up to the time of explosion.

Key words. Gamma-ray burst: individual: GRB 111117A —

1. Introduction

There is now mounting evidence that most short-duration gamma-ray bursts (GRBs) come from the merger of neutron stars (NSs), either with another NS, or a black hole, due to their apparent association with kilonovae (Barnes & Kasen 2013, Tanvir et al. 2013, Yang et al. 2015, Jin et al. 2016, Rosswog et al. 2016). The absence of associated supernovae in deep searches (e.g. Hjorth et al. 2005b, Fox et al. 2005, Hjorth et al. 2005a) supports this idea and distinguishes the physical origin of sGRBs from their long-duration counterparts. The range of host galaxy types, in some cases apparently absent, typically more massive and on average less actively star-forming than long GRB hosts (Fong et al. 2013), as well as their positions within hosts (Fong & Berger 2013), suggest an origin for the progenitors that can be very long-lived, and associated with stellar mass rather than purely star-formation rate (Berger 2014).

This progress on the progenitors of sGRBs has been enabled by localizations by the *Swift* satellite (Gehrels et al. 2009). The bulk of these localizations have associated galaxies at relatively low redshifts with a median redshift $z \sim 0.5$ (Berger 2014). Because the redshifts are measured from the hosts, measurements of the redshift distribution of sGRBs is biased towards low redshift due to cosmological dimming. So far, the electromagnetic signal from sGRBs are the only means to accurately localize NS mergers and holds the promise for detection of an associated gravitational wave signal (Ghirlanda et al. 2016). From the burst and following afterglow, modeling the properties and mapping the environments additionally allows insights into the phenomenon itself.

The total lifetimes of NS binaries is dependent on their initial separations and subsequent inspiral times, and impacts the timing and distribution of the enrichment of the ISM and subsequent stars and planets with heavy *r*-process elements (van de Voort et al. 2014, Wallner et al. 2015, Ji et al. 2016). Some limits can be calculated based on models of star-formation histories of, and the spatial distribution of sGRBs in, their host galaxies (Berger 2014). The most distant cosmological bursts, however, offer direct, hard limits.

In this *Letter* we present the spectrum of the host galaxy of the short GRB 111117A, showing it to be at higher redshift than previously estimated. We present the rest frame burst proper-

⋆ Based on observations collected at the European Southern Observatory, Paranal, Chile, Program ID: 088.A-0051 and 091.D-0904.

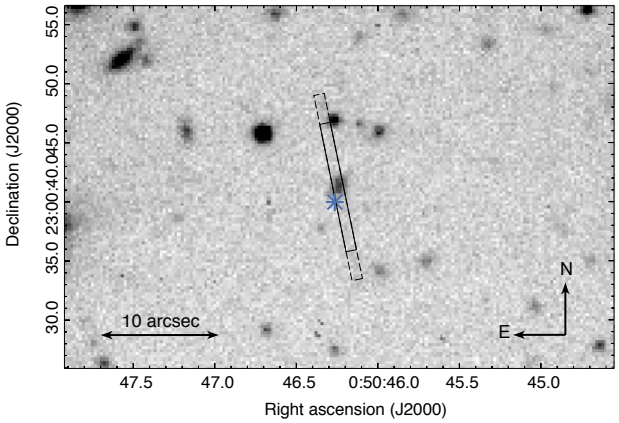

Fig. 1. Imaging of the field with the X-shooter slit overlaid. Only one slit is shown despite 4 epochs of spectroscopic observations because of the similar position angle. The image is the FORS2 R-band image, for which the photometry is shown in Fig. **??**. The blue asterisk indicates the GRB position as derived from the *Chandra* observations in Sakamoto et al. (2013)

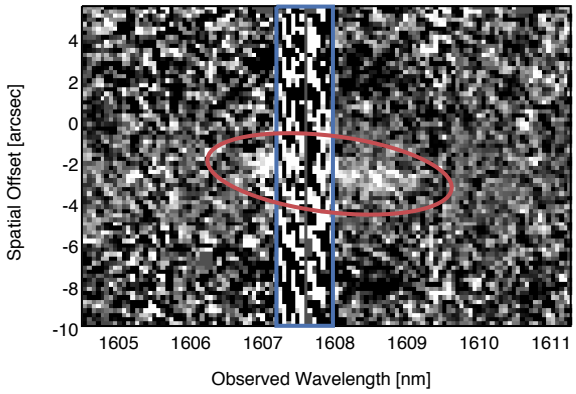

Fig. 2. 2D-image of the [O III]λ5007 emission line. The location of a bright skyline is marked by the blue box. The location of the emission line is indicated with the red ellipse. Because the host is observed in nodding-mode, negative images of the emission line appear on both sides in the spatial direction.

ties based on this new distance compared to previous analyses (Margutti et al. 2012, Sakamoto et al. 2013) and revisit the host properties derived from the new solution to the SED.

Throughout this *Letter* we use the ΛCDM cosmology provided by Planck Collaboration et al. (2016) in which the universe is flat with $H_0 = 67.7$ km s^{-1} and $\Omega_m = 0.307$ and report all magnitudes in the AB system.

2. Observations and results

2.1. Spectroscopic observations and analysis

Spectroscopic observations were carried out using the cross-dispersed echelle spectrograph, VLT/X-shooter (Vernet et al. 2011), in four seperate epochs. The burst was followed up 38 hours after the Burst Alert Telescope (BAT) trigger under ESO programme 088.A-0051 (PI: Fynbo) and again later using a different ESO program 091.D-0904 (PI: Hjorth). X-shooter can cover the wavelength range from 3000 Å to 24800 Å across three spectroscopic arms, simultaneously illuminated through the use of dichroics. The bias-correction, flat-fielding, order tracing, wavelength calibration, rectification, and flux calibration is then carried out using the VLT/X-shooter pipeline version 2.8.4 (Goldoni et al. 2006, Modigliani et al. 2010) and managed by Reflex (Freudling et al. 2013). Because the spectra are curved across each detector, a rectification algorithm is employed which introduces correlations between neighboring pixels. We select a pixel-scale of 0.2/0.2/0.6 Å/pix for the UVB/VIS/NIR arm to minimize the degree of correlation while conserving the maximal resolution. The observations are combined and extracted using scripts described in Selsing et al. 2017 (in prep.) and available online[1]. The signal-to-noise of the continuum ~~is~~ the near-infrared arm is too low to use the optimal extraction algorithm (Horne 1986), why an aperture containing the entire object has been chosen for which the flux is summed and the corresponding error is summed in quadrature. An overview of the spectroscopic observations is given in Tab. 1, and the position of the slit on the target is shown in Fig. 1.

We determine a redshift of $z = 2.211$ from from the simultaneous detection of emission lines ~~interpreted as~~ Lyα, [O II], Hβ, [O III]λ5007, and Hα, with Hβ detected at low significance ($\sim 3\sigma$). Hα only visible in the first epoch, due to the K-band blocking filter used for the remainder observations. The nebular lines exhibit a spatial extent of $\sim 1\farcs5$ and show significant velocity structure along the slit. A drop in the continuum to the blue of the Lyα line further supports the inferred redshift.

Using the integrated flux of Hα, we can infer the SFR (Kennicutt 1998, Moustakas et al. 2006). From the SED-fit, see Sect. 2.2, and the detection of Lyα the host is constrained to contain very little or no dust which is also confirmed by the shape of the spectral continuum which is why we do not apply a dust-correction. Because of the redshift, Hα falls on the far end of the NIR-arm where the night sky is very bright and additionally, several bright sky-lines intersect the line, making an accurate estimate of the Hα-flux difficult. A limit on the SFR is obtained by integrating the part of Hα free of contamination and conservatively correcting for the missing fraction by assessing the fraction integrated. Converting to a Chabrier (2003) initial mass function using Madau & Dickinson (2014) we get a limit of SFR > 7 M$_\odot$ yr^{-1}.

2.2. Imaging observations and SED analysis

We additionally imaged the field of GRB 111117A in multiple broad-band filters using the VLT equipped with FORS2 ($gRIz$ filters) and HAWK-I (JHK_s filters), long after the burst has faded. These new data are complemented by a re-analysis of some of the imagery used in Margutti et al. (2012) and Sakamoto et al. (2013) ~~that are available to us here~~ (GTC gri-band, TNG R-band, and Gemini z-band). A log of the photometric observations and measured brightness is given in Tab. 2.

All data were reduced, analyzed and fitted in a similar manner as ~~we have done previously and~~ described in detail in Krühler et al. (2011) and, ~~more recently,~~ in Schulze et al. (2016). ~~Very~~ briefly, we use our own python and IRAF routines to perform a consistent standard reduction of the available imaging which includes bias/flat-field correction, de-fringing (if necessary), sky-subtraction, and stacking of individual images for a given instrument in a given filter. The photometry of the host was tied against magnitudes of field stars from the SDSS and 2MASS catalogs in the case of $grizJHK_s$ filters. For our R and I-band photometry

[1] https://github.com/jselsing/XSGRB_reduction_scripts

we used the color transformations of Lupton[2]. We subsequently convert all magnitudes into the AB system ~~if necessary~~, and correct for the Galactic foreground of $E_{B-V} = 0.027$ mag.

The multi-color ~~spectral energy distribution (~~SED~~)~~ is then fit by Bruzual & Charlot (2003) stellar population synthesis models based on a Chabrier (2003) initial mass function in *LePhare* (Ilbert et al. 2006), where the redshift if fixed to the spectroscopic value of $z = 2.211$. The best model is obtained with an unreddened galaxy template, and returns physical parameters of luminosity ($M_B = -22.0 \pm 0.1$ mag), stellar mass ($\log(M_\star/M_\odot) = 9.9 \pm 0.2$), single stellar population age ($\tau = 0.5^{+0.5}_{-0.25}$ Gyr) and star-formation rate ($SFR_{\rm SED} = 11^{+9}_{-4} M_\odot\,{\rm yr}^{-1}$).

Noteworthy is the discrepancy of both our VLT/FORS2 photometry and the re-analysis of Gemini data to the z-band data of Margutti et al. (2012) and Sakamoto et al. (2013). Both report z-band photometry brighter by 0.8-1.0 mag than what we derive here, whereas bluer data are in excellent agreement with previously published values.

In fact, the large $i - z$ color is mistakenly interpreted as a 4000 Å break driving the galaxy photometric redshift of both of these earlier works. ~~It is this exactly this overestimate in z-band brightness that led the authors to erroneously low estimates in their photo-z~~ for GRB 111117A. Using the revised photometry from Table 2, the photo-z of the galaxy is $z_{\rm phot} = 2.04^{+0.19}_{-0.21}$, consistent with the spectroscopic value at the 1 σ confidence level.

2.3. XRT temporal and spectral analysis

We retrieved the automated data products provided by the *Swift*-XRT GRB repository[3] (Evans et al. 2009). The X-ray afterglow light curve can be fit with a single power-law decay with index $\alpha = 1.27^{+0.12}_{-0.10}$. We performed a time-integrated spectral analysis using data in photon counting (PC) mode in the widest time epoch where the $0.3 - 1.5$ keV to $1.5 - 10$ keV hardness ratio is constant (namely, from $t - T_0 = 205$ s to $t - T_0 = 203.5$ ks, for a total of 29.1 ks of data), in order to prevent spectral changes that can affect the X-ray column density determination. The obtained spectrum is well described by an absorbed power-law model. The best-fit spectral parameters are a photon index of 2.1 ± 0.4 and an intrinsic N_H of $2.4^{+2.4}_{-1.6} \times 10^{22}$ cm^{-2} ($z = 2.211$), assuming the Galactic N_H in the burst direction of 4.1×10^{20} cm^{-2}.

3. Reinterpretation of restframe properties

3.1. Classification

As already pointed out (Margutti et al. 2012, Sakamoto et al. 2013), GRB111117A very securely belongs the the short class of GRBs. Because the observed classification indicators, T_{90} and hardness ratio, do not depend strongly on redshift (Littlejohns et al. 2013), the updated redshift does not change this designation significantly. The intrinsic luminosity goes as visible in the light curve in Fig. 3, but it still is sub-luminous compared to majority of long GRBs. Bromberg et al. (2013) investigated the degree to which the long and short population distributions overlap and quantified the certainty in the class membership. GRB111117A has 96^{+3}_{-5} percent probability of being short. This is compared to the other two highest-z short candidates, GRB060121 (de Ugarte Postigo et al. 2006, Levan et al. 2006) at $1.7 \lesssim z \lesssim 4.5$ (17^{+14}_{-15} per cent) and GRB090426 (Antonelli et al. 2009, Levesque et al. 2010, Thöne et al. 2011) at $z = 2.609$ (10^{+15}_{-10} per cent).

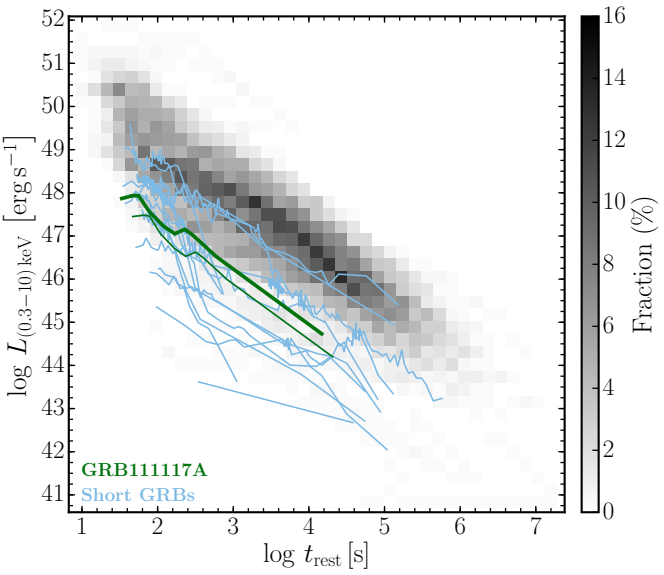

Fig. 3. Restframe XRT lightcurve of GRB111117A, compared to the general population of XRT lightcurves of GRBs. The grey shaded region is a compilation of long GRB lightcurves where the color represents density and the light blue other short GRB lightcurves for which redshifts has been determined. Despite the remarkably high redshift, the burst's luminosity is comparable to the bulk of the short burst population and still subluminous compared to the lGRB population.

3.2. Restframe N_H

We plot the recalculated N_H in Fig. 4 where we compare with the distributions of complete samples of both long and short GRBs. The long sample is from Arcodia et al. (2016) and the short sample is from D'Avanzo et al. (2014). 17 of the 99 long bursts do not have redshifts and likewise for 5 out of 16 for the short sample. Bursts without redshifts have been excluded for both groups. GRB111117A occupies a unique position in Fig. 4 with a the highest N_H of all short burst. The short sample, excluding GRB111117A, is located at low redshifts($z < 1$) and are found to populate a similar column density environment to long GRBs at similar redshifts (D'Avanzo et al. 2014). The inferred hydrogen column for GRB111117A seems to follow the trend with increasing N_H as a function of redshift as found for the long GRB hosts (Arcodia et al. 2016).

3.3. Host galaxy

From the clear host association, GRB111117A does not belong to the hostless class of GRBs (Berger 2010) and because the host exhibits clear emission lines indicative of a population of relatively young stars, as the majority of short GRBs, the host is a late-type galaxy (Fong et al. 2013). The host of GRB111117A is entirely consistent in terms of stellar mass and stellar age with the general population of short GRB hosts($\langle M_* \rangle = 10^{10.1} M_\odot$ and

[2] https://www.sdss3.org/dr8/algorithms/sdssUBVRITransform.php

[3] http://www.swift.ac.uk/xrt_products/00507901. **(Broken link, Paolo?)**

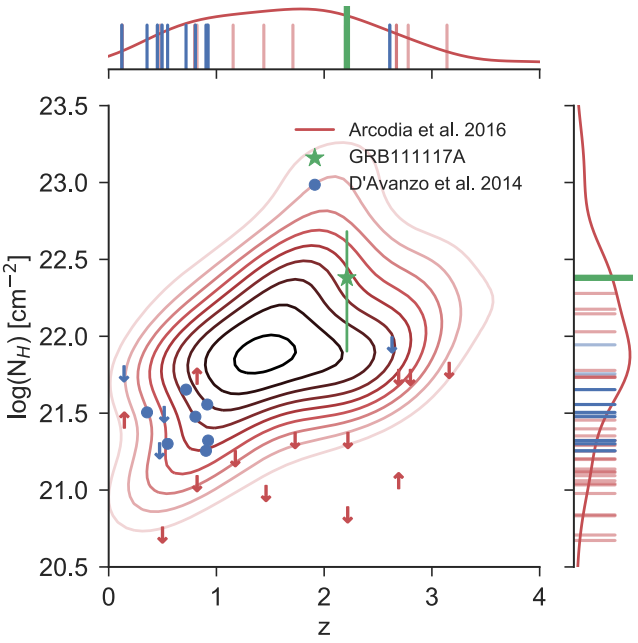

Fig. 4. Rest frame, X-ray derived hydrogen column densities for GRB111117A compared to complete samples of both long and short populations. In red is shown the long sample of Arcodia et al. (2016). The detections are replaced with contours for clarity and the limits are shown with arrows. In blue is the sample from D'Avanzo et al. (2014). GRB111117A is an outlier from the short sample, but seems to follow the distribution of long GRBs.

$\langle\tau_*\rangle$ = 0.3 Gyr) Leibler & Berger (2010). The SFR, on the other hand, is ∼1 order of magnitude higher than the typical SFR for short GRB hosts galaxies (Berger 2014) and more similar to the SFRs found in the hosts of long GRBs at a corresponding redshift (Krühler et al. 2015). Only two hosts in the sample of short GRBs compiled in Berger (2014) have a more vigorous star formation, meaning that it is in the very upper end of the star formation distribution, w[illegible]ot a complete outlie[illegible]is is likely a selection effect, because a less star-forming gala[illegible]ould exhibit weaker emission lines, thus making the redshift harder to determine. Being a late-type host, both the stellar mass and sSFR are entire[illegible]nsistent with the expected host of sGRBs(Behroozi et al. 2014). That we detect Lyα is consistent with the SED-inferred absence of dust, despite the moderate stellar age and the high X-ray derived hydrogen column density which would suggest the opposit[illegible]e centroid of the Lyα emission is found to be redshifted by [illegible] km s^{-1} with respect to systemic, which is similar to what is found for long GRB hosts (Milvang-Jensen et al. 2012) where the outflow is attributed to star formation.

4. Implications for redshift distribution of short GRBs

A single sGRB at high redshift does little in terms of constraints on the redshift distribution and therethrough the progenitor channels, but other short hosts could be missed because they are intrinsically fainter and thus this high-z event is only detected due to the brightness of the host. Berger (2014) compiled a sample of sGRB host luminosities, normalized by the characteristic galaxy luminosity at their respective redshift, $L_B/L_B^\star$. 26 out of 39 hosts (66 per cent) in the sample has redshifts. To convert the SED-inferred M_B of GRB111117A to $L_B/L_B^\star$, we use the characteristic absolute B-band magnitude of the Schechter function for the blue galaxies ($U-V < 0.25$) in the redshift window $2.0 \leq z \leq 2.5$ from Marchesini et al. (2007) and find $L_B/L_B^\star = 1.2$, which is brighter than 70 per cent of the hosts in Berger (2014) with measured $L_B/L_B^\star$. If we assume that we are able to get emission-line redshifts from hosts with $R < 25$mags (Krühler et al. 2012), then we would have missed around 30% (8 out of 26 from the sample of Berger 2014 with measured $L_B/L_B^\star$), if they were at the redshift of GRB111117A. If we assume that the hosts missing redshift in Berger (2014) follow the redshift distribution of the hosts *with* redshift, this implies that we are *not* missing a dominant fraction of sGRB redshift at $z \approx 2$, due to host faintness.

The theoretical redshift distributions of sGRBs depends on the type of delay-time function used to model the progenitor system. The redshift of GRB111117A puts constraints on the type of delay-time models suitable for modeling. The likelihood preferred lognormal time delay models investigated in Wanderman & Piran (2015) predicts a rate of sGRBs at $z = 2.211$, ∼ 2 orders of magnitude lower compared to peak rate (z = 0.9). It is stated in Wanderman & Piran (2015) that this preference depends critically on the absence of non-collapsar sGRB at $z \gtrsim 1.2$. The redshift of the burst, on the other hand, is close to the expected peak in sGRB rate calculated for the power law models (Behroozi et al. 2014, Wanderman & Piran 2015).

5. Constraints on the progenitor separation

At $z = 2.211$, the age of the universe is 2.97 Gyr. If the progenitor systems of sGRBs are the merger of two neutron stars, this sets a hard upper limit to the coalescence timescale for such a system. In the absence of other mechanisms, the timescale of the orbital decay of the system is set by the energy loss due to gravitational waves, which in turn is set by the mass of constituent compact objects and the separation of the two (Postnov & Yungelson 2014). We assume that the formation timescale of the first galaxies is short compared to the time since the big bang (Richard et al. 2011) and if we assume a mass of 1.4 $M_\odot$ for each of the neutron stars at the time of system formation, this places a limit on the initial separation of the two neutron stars of $a_0 < 3.2R_\odot$, where a_0 is the initial separation. Because we have the age of the stellar population, by using this as a limit to the orbital decay time we can put tighter constraints, $a_0 < 2.1R_\odot$, but this does not account for the possibility there could be an underlying stellar population of older stars from a previous star-formation epoch, which is why we consider $a_0 < 3.2R_\odot$ as a hard upper limit. The delay time between formation and explosion is well accomodated by the models of Belczynski et al. (2006), although the longest formation channels are excluded. This is especially true given the late type nature of the host (O'Shaughnessy et al. 2008).

6. Conclusions

We have in this letter provided a revised, spectroscopic redshift for GRB111117A based on emission lines ~~discovered using an improved reduction scheme,~~ setting it at $z = 2.211$. This value supersedes the previous photometric redshift of $z \sim 1.3$ (Margutti et al. 2012, Sakamoto et al. 2013). Part of ~~the reason for~~ the erroneous redshift estimate of previous authors is attributed to a discrepancy in the measured z-band magnitude.

The rest-frame parameters of the burst and the conditions of the burst environment have been recalculated using the new distance. The X-ray derived hydrogen column density towards

GRB111117A is the highest within a complete sample of short hosts, but seems to trace the evolution with redshift as found for the hosts of long GRBs.

The SFR of the host is in the upper end of the sGRB host SFR distribution and this plays a role in allowing a redshift to be measured for this host. Despite the moderate age and high N_H, almost no dust is present.

Although a single burst carries little leverage in terms of constraining the redshift distribution of sGRB, the high redshift of GRB111117A needs to be accommodated. A lognormal delay time model predicts a very low volumetric density of bursts at $z = 2.211$, whereas a power law delay time model peaks near GRB111117A. If more sGRBs are at this redshift, but missed due to faintness of their hosts, a lognormal delay time model will be disfavored. Compared to a sample of short hosts, GRB111117A is more luminous than 70 per cent of the sample with measured luminosities. Of the host sample, for 30 per cent, we would be unable to determine a redshift, should they be at the redshift of GRB111117A. This implies that we are *not* missing a dominant fraction of the sGRBs at $z \sim 2$.

Using the age of the universe at the time of explosion allows us to set constraints on the maximal separation between the engine constituents at the time of formation. We find that the maximal separation for two neutron stars at formation time is $a_0 < 3.2 R_\odot$, which excludes some of the formation channels with the longest timescales.

We make all the data, code and calculation related to the paper along with the paper itself available at `https://github.com/jselsing/GRB111117A`.

Acknowledgements. TK acknowledges support through the Sofja Kovalevskaja Award to P. Schady.

References

Antonelli L. A., et al., 2009, A&A, 507, L45
Arcodia R., Campana S., Salvaterra R., 2016, A&A, 590, A82
Barnes J., Kasen D., 2013, ApJ, 775, 18
Behroozi P. S., Ramirez-Ruiz E., Fryer C. L., 2014, ApJ, 792, 123
Belczynski K., Perna R., Bulik T., Kalogera V., Ivanova N., Lamb D. Q., 2006, ApJ, 648, 1110
Berger E., 2010, ApJ, 722, 1946
Berger E., 2014, ARA&A, 52, 43
Bromberg O., Nakar E., Piran T., Sari R., 2013, ApJ, 764, 179
Bruzual G., Charlot S., 2003, MNRAS, 344, 1000
Cenko S. B., Cucchiara A., 2011, GRB Coord. Network, Circ. Serv. No. 12577, #1, 12577
Chabrier G., 2003, PASP, 115, 763
Cucchiara A., Cenko S. B., 2011, GRB Coord. Network, Circ. Serv. No. 12567, #1, 12567
D'Avanzo P., et al., 2014, MNRAS, 442, 2342
Evans P. A., et al., 2009, MNRAS, 397, 1177
Fong W., Berger E., 2013, ApJ, 776, 18
Fong W., et al., 2013, ApJ, 769, 56
Fox D. B., et al., 2005, Nature, 437, 845
Freudling W., Romaniello M., Bramich D. M., Ballester P., Forchi V., García-Dabló C. E., Moehler S., Neeser M. J., 2013, A&A, 559, A96
Gehrels N., Ramirez-Ruiz E., Fox D., 2009, ARA&A, 47, 567
Ghirlanda G., et al., 2016, A&A, 594, A84
Goldoni P., Royer F., François P., Horrobin M., Blanc G., Vernet J., Modigliani A., Larsen J., 2006, Ground-based Airborne Instrum. Astron. Ed. by McLean, 6269, 80
Hjorth J., et al., 2005a, Nature, 437, 859
Hjorth J., et al., 2005b, ApJ, 630, L117
Horne K., 1986, PASP, 98, 609
Ilbert O., et al., 2006, A&A, 457, 841
Jakobsson P., Hjorth J., Fynbo J. P. U., Watson D., Pedersen K., Björnsson G., Gorosabel J., 2004, ApJ, 617, L21
Ji A. P., Frebel A., Chiti A., Simon J. D., 2016, Nature, 531, 610
Jin Z.-P., et al., 2016, Nat. Commun., 7, 12898
Jones A., Noll S., Kausch W., Szyszka C., Kimeswenger S., 2013, A&A, 560, A91
Kennicutt R. C., 1998, ARA&A, 36, 189
Krühler T., et al., 2011, A&A, 526, A153
Krühler T., et al., 2012, ApJ, 758, 46
Krühler T., et al., 2015, A&A, 581, A125
Leibler C. N., Berger E., 2010, ApJ, 725, 1202
Levan A. J., et al., 2006, ApJ, 648, L9
Levesque E. M., et al., 2010, MNRAS, 401, 963
Littlejohns O. M., Tanvir N. R., Willingale R., Evans P. A., O'Brien P. T., Levan A. J., 2013, MNRAS, 436, 3640
Madau P., Dickinson M., 2014, ARA&A, 52, 415
Marchesini D., et al., 2007, ApJ, 656, 42
Margutti R., et al., 2012, ApJ, 756, 63
Milvang-Jensen B., Fynbo J. P. U., Malesani D., Hjorth J., Jakobsson P., Møller P., 2012, ApJ, 756, 25
Modigliani A., et al., 2010, SPIE Astron. Telesc. + Instrum., 7737, 773728
Moustakas J., Kennicutt, Jr. R. C., Tremonti C. A., 2006, ApJ, 642, 775
Noll S., Kausch W., Barden M., Jones A. M., Szyszka C., Kimeswenger S., Vinther J., 2012, A&A, 543, A92
O'Shaughnessy R., Belczynski K., Kalogera V., 2008, ApJ, 675, 566
Planck Collaboration et al., 2016, A&A, 594, A13
Postnov K. A., Yungelson L. R., 2014, LRR, 17
Richard J., Kneib J.-P., Ebeling H., Stark D. P., Egami E., Fiedler A. K., 2011, Mon. Not. R. Astron. Soc. Lett., 414, L31
Rosswog S., Feindt U., Korobkin O., Wu M. R., Sollerman J., Goobar A., Martinez-Pinedo G., 2016, eprint arXiv:1611.09822
Sakamoto T., et al., 2013, ApJ, 766, 41
Schulze S., et al., 2016
Tanvir N. R., Levan A. J., Fruchter A. S., Hjorth J., Hounsell R. A., Wiersema K., Tunnicliffe R. L., 2013, Nature, 500, 547
Thöne C. C., et al., 2011, MNRAS, 414, 479
Vernet J., et al., 2011, A&A, 536, A105
Wallner A., et al., 2015, Nat. Commun., 6, 5956
Wanderman D., Piran T., 2015, MNRAS, 448, 3026
Yang B., et al., 2015, Nat. Commun., 6, 7323
de Ugarte Postigo A., et al., 2006, ApJ, 648, L83
van de Voort F., Quataert E., Hopkins P. F., Kere D., Faucher-Giguere C.-A., 2014, MNRAS, 447, 140

Table 1. Overview of the spectroscopic observations. JH in the slit width refers to observations where a K-band blocking filter has been used. The seeing is determined from the width of the spectral trace of a telluric standard star, taken close in time to the host observation. The spectral resolution, R, is measured from unresolved telluric absorption lines in the spectrum of the telluric standard star.

Obs. Date	Exposure time (s)			Slit width	Airmass	Seeing	R
	UVB	VIS	NIR	(arcsec)		(arcsec)	VIS/NIR
2011-11-19T01:33	2×2400	2×2400	8×600	1.0/1.0/0.9	1.49	0.75	11600/6700
2013-07-15T09:02	2×1200	2×1200	8×300	1.0/1.0/0.9JH	1.53	0.98	9600/8900
2013-08-03T07:37	2×1200	2×1200	8×300	1.0/1.0/0.9JH	1.55	0.85	11400/11300
2013-08-03T08:34	2×1200	2×1200	8×300	1.0/1.0/0.9JH	1.49	0.85	11400/11300

Table 2. Overview of the photometric observations.

Obs. Date	Exptime	Telescope/Instrument	Filter	Airmass	Image Quality	Host Brightness[a]
	ks				(arcsec)	($\mathrm{mag_{AB}}$)
2013-08-30T07:43	1.45	VLT/FORS2	g	1.55	0.99	24.08 ± 0.09
2011-11-17T20:07	0.80	GTC/OSIRIS	g	1.15	1.67	24.13 ± 0.09
2011-11-17T20:07	1.20	GTC/OSIRIS	r	1.11	1.50	23.93 ± 0.08
2013-07-17T08:37	1.45	VLT/FORS2	R	1.56	0.74	23.95 ± 0.06
2011-11-28T21:10	3.60	TNG/LRS	R	1.01	1.08	23.96 ± 0.13
2011-11-17T20:07	0.36	GTC/OSIRIS	i	1.08	1.50	23.89 ± 0.23
2013-08-03T09:23	1.35	VLT/FORS2	I	1.54	0.93	24.22 ± 0.15
2011-11-28T06:14	1.80	Gemini/GMOS-N	z	1.01	0.84	24.24 ± 0.47
2013-07-13T09:33	1.08	VLT/FORS2	z	1.49	0.63	23.76 ± 0.21
2013-06-24T09:14	1.98	VLT/HAWK-I	J	1.70	0.63	23.13 ± 0.18
2013-06-27T09:21	1.68	VLT/HAWK-I	H	1.63	0.91	22.94 ± 0.29
2013-06-28T09:14	1.92	VLT/HAWK-I	K_s	1.65	0.76	23.07 ± 0.32

Notes. [(a)] All magnitudes are given in the AB system and are not corrected for the expected Galactic foreground extinction corresponding to a reddening of $E_{B-V} = 0.027$ mag. **(Thomas, Can you help with the reference for the data which are not ours?)**